

Deep Learning for Predictive Analytics in Reversible Steganography

Ching-Chun Chang, Xu Wang, Sisheng Chen, Isao Echizen, *Member, IEEE*,
Victor Sanchez, *Member, IEEE*, and Chang-Tsun Li, *Senior Member, IEEE*

Abstract—Deep learning is regarded as a promising solution for reversible steganography. The recent development of end-to-end learning has made it possible to bypass multiple intermediate stages of steganographic operations with a pair of encoder and decoder neural networks. This framework is, however, incapable of guaranteeing perfect reversibility since it is difficult for this kind of monolithic machinery, in the form of a black box, to learn the intricate logics of reversible computing. A more reliable way to develop a learning-based reversible steganographic scheme is through a divide-and-conquer paradigm. Prediction-error modulation is a well-established modular framework that consists of an analytics module and a coding module. The former serves the purpose of analysing pixel correlations and predicting pixel intensities, while the latter specialises in reversible coding mechanisms. Given that reversibility is governed independently by the coding module, we narrow our focus to the incorporation of neural networks into the analytics module. The objective of this study is to evaluate the impacts of different training configurations on predictive neural networks and to provide practical insights. Context-aware pixel intensity prediction has a central role in reversible steganography and can be perceived as a low-level computer vision task. Therefore, instead of reinventing the wheel, we can adopt neural network models originally designed for such computer vision tasks to perform intensity prediction. Furthermore, we rigorously investigate the effect of intensity initialisation upon predictive performance and the influence of distributional shift in dual-layer prediction. Experimental results show that state-of-the-art steganographic performance can be achieved with advanced neural network models.

Index Terms—Deep learning, modularity, neural networks, predictive analytics, reversible steganography.

I. INTRODUCTION

ARTIFICIAL intelligence has been evolving over the years, being at the forefront of transformations of the world we live in [1]. Deep learning, as a new class of multi-purpose intelligent algorithms, learns how to solve complicated tasks through the observation of a large amount of

data, and has brought about groundbreaking advances in many branches of science [2]. The foundations of deep learning are neural networks, or connectionist systems, which are capable of discovering intricate structures in high-dimensional data via multiple layers of artificial neurons. While deep learning is currently at the very heart of multimedia technology, many research topics remain to be systematically explored.

Steganography is recognised as an important research field in multimedia forensics and security. It is the practice of concealing a message within a *cover* object to produce a *stego* object. Steganographic technology has a wide range of applications, including but not limited to covert communications, copyright protection and content authentication. Reversible steganography is used primarily for data integrity authentication by inserting an authentication code, a tamper-proof fingerprint, a hash digest or a digital signature [3]–[10]. Message embedding is carried out in a reversible manner; that is, steganographic distortion can be removed and the original data reconstructed in a time-reversed fashion.

In this era of data-centric artificial intelligence, *reversibility*, the ability to reverse a steganographic process, is a desirable feature. Secure data exchange over cyberspace is crucial for many real-world machine-learning applications for which colossal amounts of data are collected and used in the training and validation processes. However, if an irreversible steganographic algorithm is incorporated into a data exchange protocol for authentication purposes, steganographic distortion might present uncontrollable risks to the reliability of data-centric autonomous machines. It has been reported that deep-learning models are susceptible to adversarial attacks, which to some extent resemble steganographic distortion [11]–[13]. Adversarial perturbation is an invisible noise crafted to fool a deep-learning system. Adversarial contamination is to imperceptibly inject poisonous samples into the training pool, thereby compromising the accuracy of the system. Steganographic distortion resembles such an attack in the sense that both introduce an imperceptible alteration to data, although the former comes without malicious intent. Therefore, the ability to remove steganographic distortion and restore data integrity is of paramount importance.

Prediction-error modulation is one of the main pillars of contemporary reversible steganography due to its optimum rate-distortion performance [14]–[18]. A prediction-error modulation scheme has an analytics module to serve the purpose of context-aware pixel intensity prediction, and a coding module to perform encoding/decoding in the residual domain. A combination of prediction-error modulation with

This work was partially supported by KAKENHI Grants (JP16H06302, JP18H04120, JP20K23355, JP21H04907 and JP21K18023) from the Japan Society for the Promotion of Science (JSPS) and CREST Grants (JP-MJCR18A6 and JPMJCR20D3) from the Japan Science and Technology Agency (JST).

C.-C. Chang and I. Echizen are with the National Institute of Informatics, Tokyo, Japan (email: c.c.chang.phd@gmail.com; iechizen@nii.ac.jp).

X. Wang and S. Chen are with the Department of Information Engineering and Computer Science, Feng Chia University, Taichung, Taiwan. S. Chen is also with the School of Big Data and Artificial Intelligence, Fujian Polytechnic Normal University, Fuzhou, China. (email: xu.wang.phd@gmail.com; sisheng.chen.phd@gmail.com).

V. Sanchez is with the Department of Computer Science, University of Warwick, Coventry, United Kingdom (email: v.f.sanchez-silva@warwick.ac.uk).

C.-T. Li is with the School of Information Technology, Deakin University, Geelong, Australia (email: changtsun.li@deakin.edu.au).

deep learning has been described in two studies [19] and [20]. Neural networks are incorporated into the schemes based upon *modularity*. The most notable feature in common is that both studies divide pixels into *query* and *context* sets by using a chequered pattern and develop neural network models for predicting the query from the context. The main difference is neural network architectures. The former constructs a multi-scale convolutional neural network (MS-CNN) to address the issue of restricted receptive fields in traditional predictors. The latter applies a persistent memory network (MemNet) originally developed for image denoising and image super-resolution [21]. Context-aware pixel intensity prediction is closely related to such a *low-level computer vision* task in the sense that both concern low-level image features (e.g. edges, contours, and textures). Therefore, instead of reinventing the wheel, it is expected that advanced neural networks from the low-level computer vision domain can be applied directly. Another difference is that the former simply sets the query pixels to zero and learns to predict from scratch, whereas the latter initialises them to the mean of neighbouring pixels and performs prediction in a coarse-to-fine manner. It is worth investigating whether different *intensity initialisation* strategies have an impact upon predictive performance. Last but not least, the chequered pattern for context/query splitting features a dual-layer prediction: pixels assigned as the query in the first round, after partial embedding, can be assigned as the context in the second round. Such a practice gives rise to the problem of *distributional shift*—the data distribution in the target (online) domain for deployment shifts from that in the training (offline) domain. In consequence of the distortion introduced in the preceding steganographic process, assigning those distorted pixels as the context could introduce discrepancy and bias into the contextual information, thereby undermining the predictive performance. The expected performance relies on the extrapolation (generalisation) capability of neural networks. To summarise, this work aims to seek answers to the following questions:

- Can different intensity initialisation strategies affect the performance of neural networks substantially?
- Can the problem of distributional shift be mitigated, thereby enabling efficient dual-layer prediction?
- Can off-the-shelf neural networks from the low-level computer vision domain be transferred to perform pixel intensity prediction?

In this paper, we carry out empirical evaluations on several neural network models to understand the cause-effect relationships between the variables of interest. In addition to the MS-CNN and MemNet, we select three other representative low-level computer vision models for analysis: the super-resolution generative adversarial network (SRGAN) [22], the residual channel attention network (RCAN) [23] and the residual dense network (RDN) [24]. They are characterised respectively by adversarial learning, attention mechanism, and hierarchical representations. We compare zero initialisation and local-mean initialisation to gain an insight into whether pre-processing of query pixels with a local-mean filter can help the models perform better or has a counterproductive effect. Apropos of

dual-layer prediction, we explore universal training, independent training, and causal training. The universal training is to train a single model for performing prediction in both layers. The motivation is that the context/query switch can be perceived as a simple geometric translation and convolutional neural networks (CNNs) are considered to be translation-invariant. For that reason, a single model may be sufficient and can generalise well for tackling dual-layer prediction. The independent training is to train two models in parallel for respective layers. It would yield a similar result to the single-model training if our previous conjecture is valid. The causal training is to train the models in a consecutive manner such that the succeeding model is trained after the data has been modified with the preceding model. That is, a predictive model is trained and then deployed for embedding information into the training data for another model. The problem of distributional shift stems from the discrepancy between the training and deployment environments. By injecting steganographic distortion into the training data, the discrepancy may be remedied. The primary object is to minimise prediction errors and encourage a concentrated distribution of errors, thereby improving the performance of prediction-error modulation.

The remainder of this paper is organised as follows. Section II provides a literature review on the recent development of steganography with deep learning. Section III delineates modules of a reversible steganographic scheme. Section IV introduces the methodology concerning intensity initialisation strategies, dual-layer training strategies, and neural network models. Section V evaluates the impact of different variables of interest upon predictive accuracy and steganographic performance. Conclusions are drawn in Section VI.

II. LITERATURE REVIEW

The recent development of steganographic methods is centred on the use of deep-learning models to enhance performance. Significant breakthroughs have been achieved in some basic properties such as *capacity* (the allowable size of the embedded message) and *imperceptibility* (the perceptual quality of the stego object), as well as some application-oriented properties such as *secrecy* (the degree to which the stego object can elude detection), and *robustness* (the degree to which the embedded message can survive distortions of various forms) [25]. In this section, we briefly review some seminal studies of secure and robust steganography with deep learning and then discuss the use of neural networks in reversible steganography with a contrast drawn between end-to-end and modular frameworks. Note that our study focuses on the basic properties (i.e. capacity and imperceptibility) and reversibility since application-oriented requirements can be contradictory and difficult to achieve concurrently.

A. Secrecy

Secrecy is at the heart of covert communications. The ability to pass secret information under surveillance is essential to espionage and military operations. It has been reported that deep learning can be used to identify locations in a cover

image at which message embedding would not arouse suspicion [26]–[28]. More technically, a deep learning algorithm assigns a cost to every pixel to quantify the effect of making modifications. In this way, a high degree of perceptual and statistical undetectability can be reached by minimising the cost. Other approaches include using generative models to convert a given message into a cover image which is less vulnerable to steganalysis [29], to transform a cover image along with a secret message into a stego image [30], and to encode a message directly into a realistic stego image in the absence of an explicit cover image [31].

B. Robustness

Robustness is a prioritised requirement for copyright protection. In commercial applications, entrepreneurs can prevent copyright infringement by embedding a registered watermark into digital assets. Deep learning has been used to embed invisible watermarks into images and videos in a durable way in order to identify copyright ownership and deter illegitimate copying [32]. Unauthorised screen recording is a new scenario in which an adversary attempts to capture an electronically displayed still photograph or video footage with a digital camera, causing optical interference in watermark extraction. It has been shown that neural networks can be trained to simulate optical interference and then learn to encode and decode watermarks in a robust manner [33]. Decoding accuracy can also be enhanced by using neural networks to remove light artefacts such as moiré fringes, a type of textile with a rippled or wavy appearance, prior to watermark extraction [34]. To facilitate augmented reality, deep learning has been used to decode hyperlinks embedded in physical photographs rather than digital media, subject to real-world variations in print quality, illumination, occlusion and viewing distance [35].

C. Reversibility—End-to-End Framework

Reversibility is a desirable characteristic for applications in which accuracy and consistency of data are important. It is a requisite for preventing an accumulation of steganographic distortion over each data transmission. In contrast to the rapid development of deep-learning-based irreversible steganography, the use of deep neural networks in reversible steganography remains largely unexplored. A reversible steganographic method often relies on intricate logical operations to regulate imperceptibility and guarantee reversibility. Such operations are hard to achieve using existing neural network models. One of the earliest approaches uses a U-shaped network (U-Net) to automatically encode a cover image and a secret message into a stego image and a separate neural network model for decoding [36]. Another approach encodes a message bitstream into a cover image via a generative model, trains a cycle-consistent generative adversarial network (CycleGAN) to learn the back-and-forth transformation between the cover and stego images, and extracts the message bitstream from the stego image by using another neural network model [37]. Furthermore, an intriguing study shows that both encoding (forward mapping) and decoding (inverse mapping) can be performed by using a single invertible neural network (INN) [38].

While a monolithic end-to-end system generally offers a large steganographic capacity, a common limitation within this type of framework is imperfect reversibility due to the presence of an information bottleneck (i.e. a form of lossy compression) in neural networks. The lack of transparency, interpretability and explainability in neural networks adds an extra dimension to the problem.

D. Reversibility—Modular Framework

Although reversibility is not an all-or-nothing proposition, the unreliability of end-to-end learning may pose uncontrollable risks in certain circumstances. Problem decomposition or modularisation is essential to addressing complex problems. Existing reversible steganographic schemes often consist of *coding* and *analytics* modules. In general, the coding module handles the encoding and decoding mechanisms, which are designed to achieve perfect reversibility subject to an imperceptibility constraint. The analytics module models the data distribution and exploits data redundancy in order to optimise steganographic rate-distortion performance. For instance, the regular–singular (RS) scheme introduced by Fridrich *et al.* constructs a discrimination function to categorise image blocks into regular, singular and unusable groups on the basis of the smoothness prior, and uses invertible flipping of the least significant bits to achieve invisible and erasable embedding [39]. We can define the former part as the analytics module and the latter part as the coding module. The problem of limited reversibility in previous deep-learning approaches lies in the difficulty of lossless coding in an end-to-end learning fashion. A recent study achieves perfect reversibility with a deep-learning-based RS scheme following this established *modular* framework [40]. A conditional generative adversarial network (GAN), referred to as pix2pix [41], is applied to improve the performance of the discrimination function. It has been shown that by partitioning a scheme into coding and analytics modules and deploying neural networks in the latter, reversibility can be reliably guaranteed.

III. REVERSIBLE STEGANOGRAPHY

In this section, we delineate a reversible steganographic scheme based on prediction-error modulation. We begin with an overview of the scheme and then dissect each scheme component.

A. Scheme Overview

A schematic workflow of the encoding and decoding procedures is provided in Figure 1 with the definitions of variables and operations listed in Table I. The scheme based on prediction-error modulation can be broken down into an analytics module and a coding module. The former models the distribution of natural images and predicts the intensity of query pixels on the basis of the available context pixels. The latter encodes/decodes messages into/from prediction errors. Consider the following scenario: A sender (encoder) embeds a message m into a cover image x to produce a stego image x' and then transmits it to a receiver (decoder) who extracts

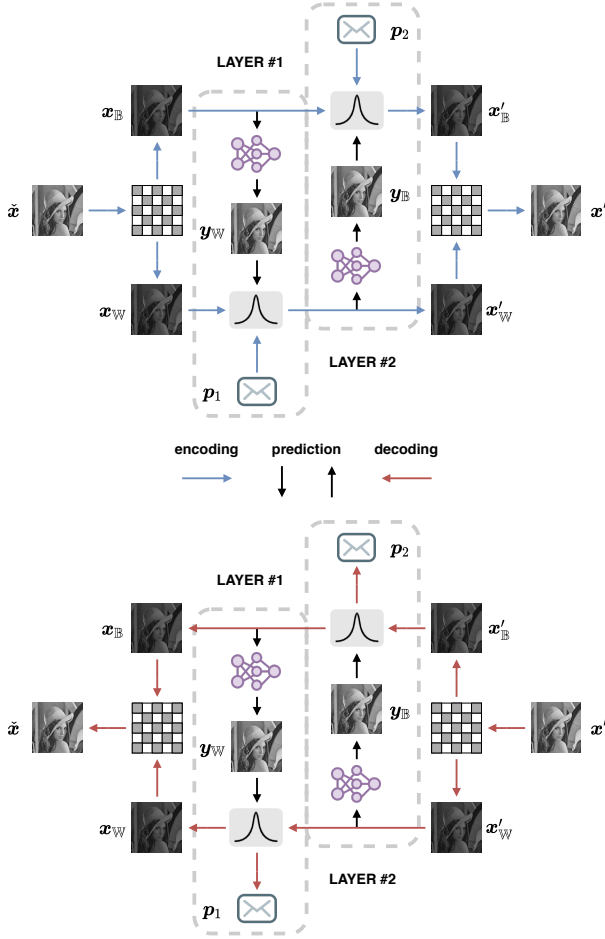


Fig. 1: Schematic workflow of encoding and decoding procedures.

the message and restores the cover image on receipt of the stego image.

At the encoder side, we pre-process the cover image to prevent pixel intensity overflow during message embedding at the cost of generating extra auxiliary information. We treat the auxiliary information as a part of the payload and concatenate it with the intended message. Then, a chequered pattern is applied to split the image into a black set and a white set of pixels, denoted respectively by x_B and x_W . In the first-layer prediction, we designate the black set as the context set and the white set as the query set. The roles are reversed in the second-layer prediction. We make use of a neural network or a predictive algorithm to estimate the intensities of the query pixels based on the observed context pixels. The prediction errors or residuals, denoted by ε , are computed by subtracting the predicted values from the actual values. A portion of the payload is embedded in the residual domain through arithmetic operations. The modulated prediction errors, denoted by ε' , are then added to the predicted values, resulting in a slight distortion to the query pixels. The process can be repeated once more to embed another part of the payload by swapping the roles between the context and the query.

At the decoder side, we carry out message extraction and image restoration in a *last-in-first-out* manner. Similar to the encoding process, the decoding process begins by splitting

TABLE I: List of variables and operations.

var. & op.	definition
x	cover image
x'	stego image
\tilde{x}	processed image
x_C	context pixels
x_Q	query pixels
y_Q	predicted query pixels (predicted image)
ε	prediction errors
ε'	modulated prediction errors
v	overflow-status register
m	message
p	payload
ϑ	stego-channel parameter
\mathbb{B}	black set of pixel coordinates
\mathbb{W}	white set of pixel coordinates
net_1	neural network for first-layer prediction
net_2	neural network for second-layer prediction
$scale_{\downarrow}$	downscaling of possibly overflowing pixels
$scale_{\uparrow}$	upscaling of possibly overflowing pixels
split	context-query splitting
merge	context-query merger
encode	prediction-error modulation (payload embedding)
decode	prediction-error de-modulation (payload extraction)
concat	concatenation of bit-streams
deconcat	de-concatenation of bit-streams

pixels of the stego image into the context and the query, predicting the query from the context, and calculating the prediction errors. A partial payload is extracted and the prediction errors are de-modulated back to the original state through inverse operations. Steganographic distortion is removed by adding the restored prediction errors to the predicted values. The decoding process can likewise be repeated once more by swapping roles between the context and query. Finally, the restored image is post-processed with the extracted auxiliary information to undo the minute modifications caused by the overflow prevention measure.

To summarise, the algorithmic steps are enumerated as follows. For the encoding phase:

- 1) $\{\tilde{x}, v\} = scale_{\downarrow}(x)$;
- 2) $p = concat(v, m)$;
- 3) $\{x_B, x_W\} = split(\tilde{x})$;
- 4) $y_W = net_1(x_B)$;
- 5) $x'_W = encode(x_W, y_W, p_1 | Q = \mathbb{W})$;
- 6) $y_B = net_2(x'_W)$;
- 7) $x'_B = encode(x_B, y_B, p_2 | Q = \mathbb{B})$;
- 8) $x' = merge(x'_B, x'_W)$.

For the decoding phase:

- 1) $(x'_B, x'_W) = split(x')$;
- 2) $y_B = net_2(x'_W)$;
- 3) $\{x_B, p_2\} = decode(x'_B, y_B | Q = \mathbb{B})$;
- 4) $y_W = net_1(x_B)$;
- 5) $\{x_W, p_1\} = decode(x'_W, y_W | Q = \mathbb{W})$;
- 6) $\tilde{x} = merge(x_B, x_W)$;
- 7) $\{v, m\} = deconcat(p)$;
- 8) $x = scale_{\uparrow}(\tilde{x}, v)$.

All images are assumed to be 8-bit greyscale throughout this study. Let us denote by ϑ a threshold for the stego channel such that

$$\text{stego channel: } \{\varepsilon \mid \text{abs}(\varepsilon) < \vartheta\}, \quad (1)$$

Algorithm 1 Down-scaling

Input: x, ϑ
Output: \tilde{x}, v
 \triangleright down-scaling
 $v = \emptyset$
for $i \leftarrow 1$ to $\text{height}(x)$ **do**
 for $j \leftarrow 1$ to $\text{width}(x)$ **do**
 $\tilde{x}_{i,j} \leftarrow x_{i,j}$
 if $x_{i,j} \geq 255 - \vartheta + 1$ **then** \triangleright overflow
 $\tilde{x}_{i,j} \leftarrow x_{i,j} - \vartheta$
 $v = \text{concat}(v, 1)$
 else if $255 - \vartheta \geq x_{i,j} \geq 255 - 2\vartheta + 1$ **then**
 $v = \text{concat}(v, 0)$
 else if $x_t \leq 0 + \vartheta - 1$ **then** \triangleright overflow
 $\tilde{x}_{i,j} \leftarrow x_{i,j} + \vartheta$
 $v = \text{concat}(v, 1)$
 else if $0 + \vartheta \leq x_t \leq 0 + 2\vartheta - 1$ **then**
 $v = \text{concat}(v, 0)$

TABLE II: Code charts for overflow prevention w.r.t. different settings of ϑ .**(a)** $\vartheta = 1$

x	0	255
\tilde{x}	1	254

(b) $\vartheta = 2$

x	0	1	254	255
\tilde{x}	2	3	252	253

(c) $\vartheta = 3$

x	0	1	2	253	254	255
\tilde{x}	3	4	5	250	251	252

where abs denotes the absolute value. In other words, we use the parameter ϑ to determine for which prediction error values the payload embedding process can take place. The following presents the algorithmic details surrounding the notion of the stego channel.

B. Overflow Handling

Both encoding and decoding are carried out in the residual domain. Addition and subtraction on residual values are equivalent to the same arithmetic operations on pixel values (i.e. a pro rata increment or decrement in pixel intensity). Given that computations are defined in a Galois finite field, such arithmetic operations may cause pixel intensity overflow: intensity values that are unexpectedly small or large wrap around the minimum or maximum after manipulations. We pre-process the image to prevent pixels from moving off boundary (or becoming saturated) and mark the locations where off-boundary pixels may occur. To distinguish between the processed pixels \tilde{x} and unprocessed pixels x with the same value, we flag 1 (true) for the former and 0 (false) for the latter

Algorithm 2 Up-scaling

Input: \tilde{x}, v, ϑ
Output: x
 \triangleright up-scaling
 $t = 1$
for $i \leftarrow 1$ to $\text{height}(\tilde{x})$ **do**
 for $j \leftarrow 1$ to $\text{width}(\tilde{x})$ **do**
 $x_{i,j} \leftarrow \tilde{x}_{i,j}$
 if $255 - \vartheta \geq x_{i,j} \geq 255 - 2\vartheta + 1$ **then**
 if $v_t = 1$ **then** \triangleright overflow
 $x_{i,j} \leftarrow \tilde{x}_{i,j} + \vartheta$
 $t = t + 1$
 else if $0 + \vartheta \leq x_{i,j} \leq 0 + 2\vartheta - 1$ **then**
 if $v_t = 1$ **then** \triangleright overflow
 $\tilde{x}_{i,j} \leftarrow x_{i,j} - \vartheta$
 $t = t + 1$;

in an overflow-status register, that is,

$$\tilde{x}_{i,j} = \begin{cases} x_{i,j} + \vartheta & \text{if } x_{i,j} \in \mathbb{L}_1, \\ x_{i,j} - \vartheta & \text{if } x_{i,j} \in \mathbb{U}_1, \\ x_{i,j} & \text{otherwise,} \end{cases} \quad (2)$$

and

$$v = \begin{cases} \text{concat}(v, 0) & \text{if } x_{i,j} \in \mathbb{L}_0 \cup \mathbb{U}_0, \\ \text{concat}(v, 1) & \text{if } x_{i,j} \in \mathbb{L}_1 \cup \mathbb{U}_1, \end{cases} \quad (3)$$

where

$$\begin{aligned} \mathbb{L}_0 &= [0 + \vartheta, 0 + 2\vartheta - 1], \\ \mathbb{L}_1 &= [0, 0 + \vartheta - 1], \\ \mathbb{U}_0 &= [255 - 2\vartheta + 1, 255 - \vartheta], \\ \mathbb{U}_1 &= [255 - \vartheta + 1, 255]. \end{aligned} \quad (4)$$

The parameter ϑ is associated with the modulation step in the message embedding process. A greater value of ϑ spans a wider range of pixel values that may be modified beyond the boundary and thus having a higher probability of increasing the size of the register. The overflow-status register is an overhead of reversibility. It has to be concatenated with the message and embedded as a part of the payload. As a consequence, its size has to be deducted from the overall payload when assessing steganographic capacity. See Algorithms 1 and 2 for the pseudo-codes. The overflow handling process is codified in Table II.

C. Context/Query Splitting

A convenient way to define pixel connectivity is to consider the von Neumann neighbourhood, that is, four adjacent pixels connected horizontally and vertically. If we sample the context and query pixels uniformly in such a way that each query pixel has 4 connected context pixels, we end up forming a pattern analogous to a chequerboard, as illustrated in Figure 2. We

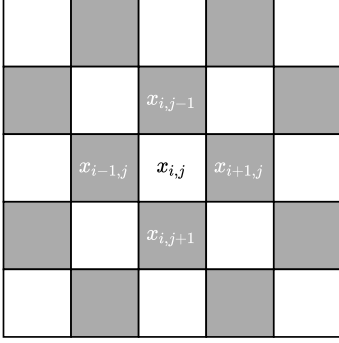


Fig. 2: Illustration of chequered pattern for context-query splitting.

can define the black set \mathbb{B} as the context and the white set \mathbb{W} as the query (or the other way round):

$$(i, j) \in \begin{cases} \mathbb{B} := \mathcal{C} & \text{if } i + j \text{ is odd,} \\ \mathbb{W} := \mathcal{Q} & \text{if } i + j \text{ is even.} \end{cases} \quad (5)$$

A naïve way to estimate the intensity of the central pixel is to calculate the mean of locally connected pixels. This linear predictive model, referred to as local-mean interpolation (LMI) [42], is based on the smoothness prior, a generic contextual constraint on real-world photographs. The question of how to improve upon the predictive accuracy is a primary concern of this study and this is where deep learning comes in.

D. Encoding/Decoding

Let $y_{i,j}$ denote a prediction of the pixel at location (i, j) . For each query pixel, we compute its prediction error by

$$\varepsilon = \tilde{x}_{i,j} - y_{i,j}. \quad (6)$$

For the prediction errors determined as the stego channel, we embed a bit of payload information by

$$\varepsilon' = \varepsilon + \text{sgn}(\varepsilon) \cdot p_t, \quad (7)$$

where sgn extracts the sign of the prediction error (either positive or negative) and p_t is the current payload bit. For the rest of the errors, we shift them by ϑ to prevent error values from overlapping (i.e. indistinguishable from the errors determined as stego channel); that is,

$$\varepsilon' = \varepsilon + \text{sgn}(\varepsilon) \cdot \vartheta. \quad (8)$$

A modulated error is then added to the predicted value, resulting in a stego pixel

$$x'_{i,j} = y_{i,j} + \varepsilon'. \quad (9)$$

Let us take the case in which $\vartheta = 2$ for example. When $\varepsilon = 0$, we can map it to one of the three states, $\varepsilon' = 0$ or ± 1 , to encode a ternary digit (a trit of information). When $\varepsilon = \pm 1$, we shift it to ± 2 to avoid ambiguity and map it to one of the two states, $\varepsilon' = \pm 2$ or ± 3 (disregarding the sign), to represent one bit of information. For all other ε such that $\varepsilon \notin (-\vartheta, +\vartheta)$, we shift each of them by ϑ in either a positive or negative direction, depending on the sign. However, converting the payload between binary (base 2) and ternary

(base 3) numeral systems on the fly can be problematic. To circumvent this issue, we can map the errors with value 0 to the digit 0 if the observed payload bit p_t is 0₂; otherwise, we read the next payload bit p_{t+1} and map the errors to the digit -1 if $[p_t, p_{t+1}] = [1_2, 0_2]$ and to the digit $+1$ if $[p_t, p_{t+1}] = [1_2, 1_2]$; that is,

$$\{\varepsilon' \mid \varepsilon = 0\} = \begin{cases} 0 & \text{if } p_t = 0_2, \\ -1 & \text{if } [p_t, p_{t+1}] = [1_2, 0_2], \\ +1 & \text{if } [p_t, p_{t+1}] = [1_2, 1_2]. \end{cases} \quad (10)$$

Theoretically, the mapping permits one trit or $\log_2 3 \approx 1.585$ bits of information to be embedded. In practice, the compromised solution embeds one or two bits with a probability of 0.5 each, thereby being capable of embedding 1.5 bits on average for $\varepsilon = 0$. Decoding is simply an inverse mapping. It begins by predicting the query pixel intensities and computing the prediction errors. Each error is de-modulated according to its magnitude. For errors between ± 1 , we map them back to 0 and extract the corresponding payload bits. For errors whose magnitude is in $(1, 2\vartheta)$ regardless of the sign, we de-modulate them by the floor division of the magnitude by 2 and extract the payload bits by the remainder of the division. For the rest errors, we shift them back by ϑ . The original pixel intensity is recovered by adding the de-modulated error to the predicted value. According to the *Law of Error* [43], we can hypothesise that the frequency of an error approximates an exponential function of its magnitude and therefore follows a zero-mean Laplacian distribution. This symmetrical modulation pattern is derived from the fact that prediction errors are expected to centre around 0. Therefore, it is advisable to designate errors with a small absolute magnitude (of high frequency) as the stego channel. A rise in the width of the stego channel represents an increased steganographic capacity. See Algorithms 3 and 4 for the pseudo-codes. The prediction-error modulation process is codified in Table III. We would like to note that this coding method is simple, readily scalable and computationally efficient but not necessarily optimal. The main theme of this study is the analytics module, which is independent of the coding module. Any coding method that reflects more accurately the statistical distribution of residuals can be applied without conflicting with the findings of this study.

IV. PREDICTIVE ANALYTICS

In this section, we take a closer look at the practice of training neural networks for predictive analytics in reversible steganography. We investigate different initialisation strategies for configuring the inputs of neural networks, different training strategies for fitting neural networks with dual-layer prediction, and different neural network architectures suitable for context-aware pixel intensity prediction.

A. Initialisation Strategies

Recall that the first step of the encoding phase is to split a cover image into two sub-images: $(x_{\mathbb{B}}, x_{\mathbb{W}}) = \text{split}(x)$. Note that we use x instead of \tilde{x} here because the distortion caused by pre-processing is generally negligible. While our goal is to

Algorithm 3 Modulation

Input: $\varepsilon, p, t, \vartheta$
Output: ε', t

▷ modulation

if $\varepsilon = 0$ **then**

if $p_t = 0$ **then** ▷ embed 1 bit

$\varepsilon' \leftarrow 0$

$t \leftarrow t + 1$

else if $p_t = 1$ and $p_{t+1} = 0$ **then** ▷ embed 2 bits

$\varepsilon' \leftarrow -1$

$t \leftarrow t + 2$

else if $p_t = 1$ and $p_{t+1} = 1$ **then** ▷ embed 2 bits

$\varepsilon' \leftarrow +1$

$t \leftarrow t + 2$

else if $0 < \text{abs}(\varepsilon) < \vartheta$ **then** ▷ embed 1 bit

if $p_t = 0$ **then**

$\varepsilon' \leftarrow 2\varepsilon$

else

$\varepsilon' \leftarrow 2\varepsilon + \text{sgn}(\varepsilon) \cdot 1$

$t \leftarrow t + 1$

else ▷ non-embeddable

$\varepsilon' \leftarrow \varepsilon + \text{sgn}(\varepsilon) \cdot \vartheta$

$t \leftarrow t$

Algorithm 4 De-modulation

Input: $\varepsilon', p, t, \vartheta$
Output: ε, p, t

▷ de-modulation

if $0 \leq \text{abs}(\varepsilon') \leq 1$ **then**

$\varepsilon \leftarrow 0$

if $\varepsilon' = 0$ **then** ▷ extract 1 bit

$p \leftarrow \text{concat}(p, 0)$

$t \leftarrow t + 1$

else if $\varepsilon' = -1$ **then** ▷ extract 2 bits

$p \leftarrow \text{concat}(p, 1, 0)$

$t \leftarrow t + 2$

else if $\varepsilon' = +1$ **then** ▷ extract 2 bits

$p \leftarrow \text{concat}(p, 1, 1)$

$t \leftarrow t + 2$

else if $1 < \text{abs}(\varepsilon') < 2\vartheta$ **then** ▷ extract 1 bit

$\varepsilon \leftarrow \text{floor}(\text{abs}(\varepsilon')/2) \cdot \text{sgn}(\varepsilon')$

$p \leftarrow \text{concat}(p, \text{mod}(\text{abs}(\varepsilon'), 2))$

$t \leftarrow t + 1$

else ▷ non-extractable

$\varepsilon \leftarrow \varepsilon' - \text{sgn}(\varepsilon') \cdot \vartheta$

$p \leftarrow p$

$t \leftarrow t$

TABLE III: Code charts for prediction-error modulation w.r.t. different settings of ϑ .(a) $\vartheta = 1$

ε	-254	...	-3	-2	-1	0	0	0	+1	+2	+3	...	+254
p	\emptyset	...	\emptyset	\emptyset	\emptyset	10 ₂	0 ₂	11 ₂	\emptyset	\emptyset	\emptyset	...	\emptyset
ε'	-255	...	-4	-3	-2	-1	0	+1	+2	+3	+4	...	+255

(b) $\vartheta = 2$

ε	-253	...	-3	-2	-1	0	0	0	+1	+2	+3	...	+253
p	\emptyset	...	\emptyset	\emptyset	1 ₂	0 ₂	10 ₂	0 ₂	11 ₂	0 ₂	1 ₂	\emptyset	\emptyset
ε'	-255	...	-5	-4	-3	-2	-1	0	+1	+2	+3	+4	+5

(c) $\vartheta = 3$

ε	-252	...	-3	-2	-1	0	0	0	+1	+2	+3	...	+252
p	\emptyset	...	\emptyset	1 ₂	0 ₂	1 ₂	0 ₂	10 ₂	0 ₂	11 ₂	0 ₂	1 ₂	\emptyset
ε'	-255	...	-6	-5	-4	-3	-2	-1	0	+1	+2	+3	+4

predict the intensities of query pixels, we have to determine the initial value of each query pixel in $\mathbf{x}_{\mathbb{B}}$ and $\mathbf{x}_{\mathbb{W}}$ since the input to the applied neural networks must be a complete image. To this end, we consider two simple initialisation strategies: zero initialisation and local-mean initialisation.

1) *Zero initialisation:* For zero initialisation, we set the initial value for each query pixel to 0 and preserve the context pixels, as given by

$$\mathbf{x}_{\mathcal{C}} = \text{init}(\mathbf{x} \mid \mathcal{C}) = \begin{cases} 0 & \text{if } (i, j) \in \mathcal{Q}, \\ x_{i,j} & \text{if } (i, j) \in \mathcal{C}. \end{cases} \quad (11)$$

This strategy is rather arbitrary but computationally efficient when compared with other initialisation strategies. Apart from this, it involves little subjective knowledge, preliminary analysis, or preconception about the intensities. Therefore, it might minimise the interference in the learning process.

2) *Local-mean initialisation:* For local-mean initialisation, we assign the mean intensity of 4 connected neighbours denoted by $\bar{x}_{i,j}$ as the initial value of each query pixel; that is,

$$\mathbf{x}_{\mathcal{C}} = \text{init}(\mathbf{x} \mid \mathcal{C}) = \begin{cases} \bar{x}_{i,j} & \text{if } (i, j) \in \mathcal{Q}, \\ x_{i,j} & \text{if } (i, j) \in \mathcal{C}. \end{cases} \quad (12)$$

This strategy involves the computation of a local mean, but it is often the case that pre-estimation could help to accelerate the training process. Learning-based models tend to perform better and converge faster when such approximate values are pre-calculated.

B. Training Strategies

Dual-layer prediction entails the problem of distributional shift because steganographic distortion appears after the first-layer embedding. In the first layer, the intensities of query

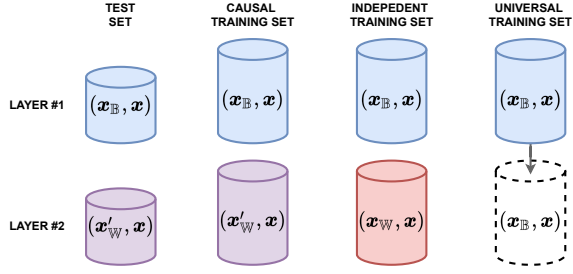


Fig. 3: Illustration of training/test set division.

pixels are predicted by a neural network model and then modified with the prediction-error modulation algorithm. In the second layer, the roles of context and query are switched. As a result, the context set consists of distorted pixels. This can also be viewed as uncertainty propagation in the sense that errors in the previous layer propagate to the next layer, impairing the predictive performance. Formally, we aim to minimise the loss of two test sets:

$$\begin{aligned} \text{test}_1 &: \mathcal{L}(\text{net}(\mathbf{x}_B), \mathbf{x}), \\ \text{test}_2 &: \mathcal{L}(\text{net}(\mathbf{x}'_W), \mathbf{x}). \end{aligned} \quad (13)$$

To this end, we explore three training strategies: universal training, independent training, and causal training. The training strategies differ by the configurations of the training set, as illustrated in Figure 3.

1) *Universal training*: A cost-efficient way to manage dual-layer prediction is to train a single predictive model. The context/query switch between the first and second layers can be viewed as a geometric translation. According to the chequered pattern, the context (or query) coordinates of the first layer, when shifted by one step (either horizontally or vertically), becomes the context (or query) coordinates of the second layer. Inspired by the translation-invariance property of classic CNN models, we conjecture that a model trained on the first set can be deployed directly to make inferences on the second test set. In other words, for both test sets, we train a universal model by

$$\text{net}_{\text{uni}} : \underset{\text{net}}{\text{argmin}} \mathcal{L}(\text{net}(\mathbf{x}_B), \mathbf{x}). \quad (14)$$

2) *Independent training*: Another way to accommodate dual-layer prediction is to train two independent predictive models. For inference on the second test set, we structure the training set without taking account of steganographic distortion. This strategy can serve to check whether a single translation-invariant model is adequate. If the conjecture is valid, both would yield a similar result. Although the practice of training two models indicates an extra computational cost, this strategy permits parallel training because the unmodified images rather than stego images are used as the inputs for training the second-layer predictor, that is,

$$\begin{aligned} \text{net}_{\text{ind}}^1 &: \underset{\text{net}}{\text{argmin}} \mathcal{L}(\text{net}(\mathbf{x}_B), \mathbf{x}), \\ \text{net}_{\text{ind}}^2 &: \underset{\text{net}}{\text{argmin}} \mathcal{L}(\text{net}(\mathbf{x}_W), \mathbf{x}). \end{aligned} \quad (15)$$

3) *Causal training*: The cause of the distributional shift is the discrepancy between the distributions of the training

and test sets. Reducing the deployment loss requires the distribution of the training set to be as close as possible to that of the test set. A potential way to alleviate the problem is to add steganographic distortion to the second-layer training set. While the distortion varies with the embedded message (rather than being a fixed pattern), we hypothesis that neural networks can learn to predict from a much more stable and reliable image representation if such distortion is presented during training. Implementing a steganographic algorithm incurs an extra computational cost and the succeeding model can only be trained once the training of the preceding model has been completed. Two models are causally connected as the prediction of the first model contributes to the prediction of the second model. Specifically, two models are trained by

$$\begin{aligned} \text{net}_{\text{cos}}^1 &: \underset{\text{net}}{\text{argmin}} \mathcal{L}(\text{net}(\mathbf{x}_B), \mathbf{x}), \\ \text{net}_{\text{cos}}^2 &: \underset{\text{net}}{\text{argmin}} \mathcal{L}(\text{net}(\mathbf{x}'_W), \mathbf{x}). \end{aligned} \quad (16)$$

C. Neural Networks

Based on the perception that context-aware pixel intensity prediction is closely associated with low-level computer vision, we adopt advanced deep-learning models originally devised for image denoising and image super-resolution. The goal is to refine a given prior (noisy and low-resolution) reference image into a posterior (clean and high-resolution) reference image through a neural network: $\mathbf{y} = \text{net}(\mathbf{x})$. A neural network can be perceived as a non-linear function that learns to minimise a pre-defined loss function by transforming the input into useful features or representations in a latent space. In this sense, the terms feature, representation, and latent state are used interchangeably hereinafter. Note that each implemented neural network may involve minor modifications to its original version. In particular, upsampling and transposed convolutional layers are replaced with regular convolutional layers. To ensure reproducibility, the architectural details of the five models used for empirical evaluation are illustrated in Figure 4 and specified as follows.

1) *MS-CNN*: The MS-CNN extracts multi-scale image features with convolutional kernels of different sizes parallel to one another, to overcome the problem of restricted receptive fields in traditional linear predictors. The multi-scale features are aggregated in two successive convolutional layers to make a final prediction. In the implementation, the multi-scale kernel sizes are configured to 3×3 , 5×5 , and 7×7 with the number of channels set to 32. The activation function involved is a leaky rectified linear unit (LeakyReLU) [44]. The model is trained to minimise the ℓ_1 norm.

2) *MemNet*: The MemNet consists of interconnected memory cells, each comprising a recurrent unit and a gate unit. The recurrent connectivity substantially reduces the number of trainable parameters, enabling the formation of a lightweight model for storage. The gating mechanism regulates important latent states or persistent memories, thereby mitigating the vanishing gradient problem often encountered when training deep neural networks. The recurrent unit comprises a series of residual blocks with shared weights, whereas the gating mechanism is a convolutional layer with a kernel size of 1×1 .

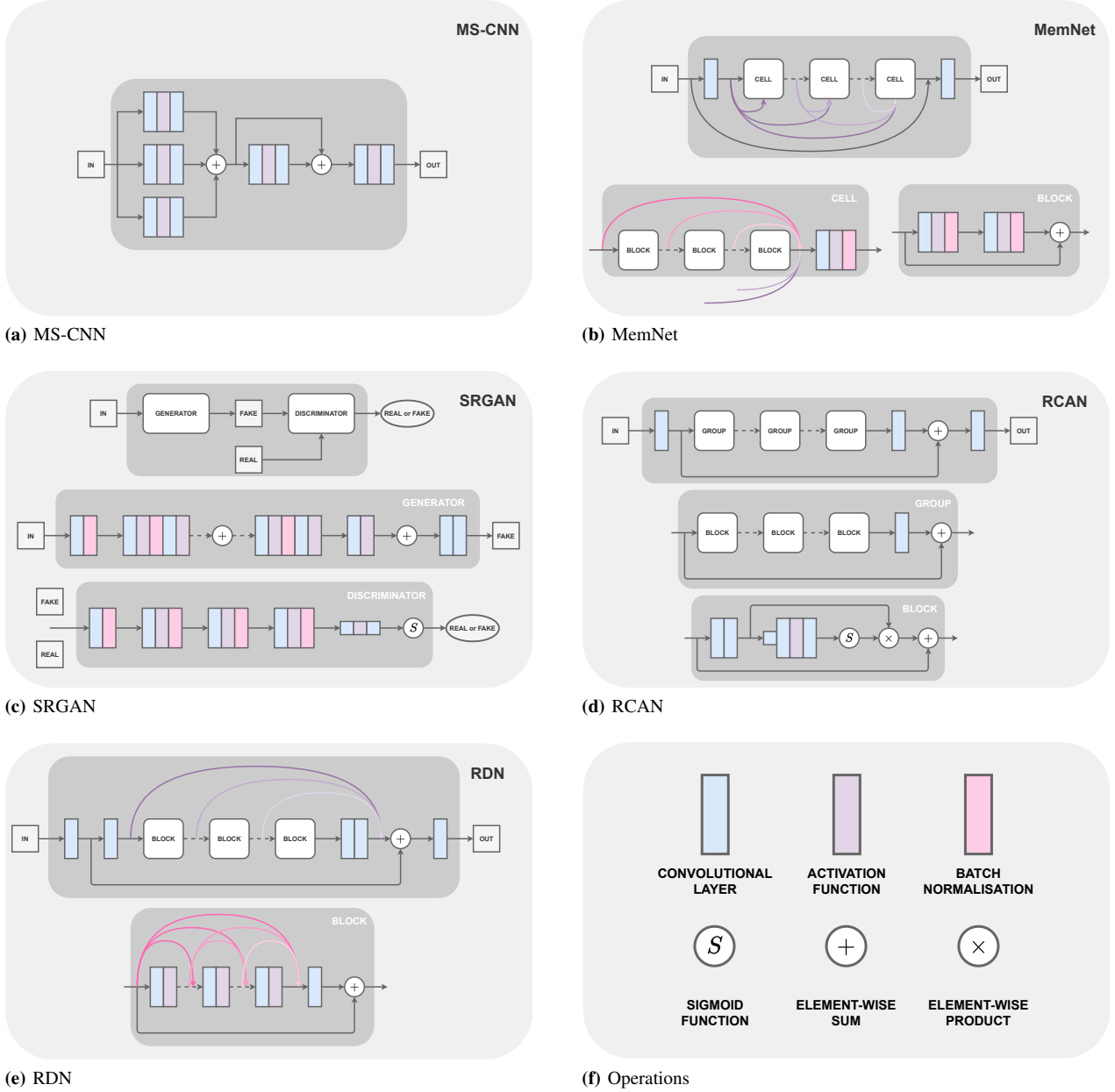


Fig. 4: Architectural details of deep neural network models.

For each memory cell, the outputs from the tightly structured residual blocks (short-term memories) along with the outputs from previous cells pass through a gate unit to attain a persistent state (long-term memory). In the implementation, the number of memory cells and the number of residual blocks in each cell are both configured to 5 with the kernel size set to 3×3 and the number of channels set to 64. The non-linear activation function involved is a rectified linear unit (ReLU) [45]. The model is trained to minimise the ℓ_1 norm.

3) *SRGAN*: The SRGAN has a generator and a discriminator trained to converge to a Nash equilibrium. The goal assigned to the generator is to fool the discriminator by generating realistic images and conversely the goal assigned to the discriminator is to tell apart fake and real images. The generator comprises residual blocks with skip connections, and

the discriminator consists of strided convolutions to reduce the dimensionality followed by two dense (fully connected) layers and a sigmoid activation function for estimating the probability of real/fake classification. In the implementation, the number of residual blocks is configured to 5 with the kernel size set to 3×3 and the number of channels set to 64. The non-linear activation function involved in the generator is a parametric rectified linear unit (PReLU) [46]. The model is trained to minimise a weighted loss function composed of the ℓ_2 norm, the perceptual loss and the adversarial loss. The perceptual loss is computed based on the Euclidean distance between the feature maps extracted by a pre-trained 19-layer VGG network [47] and the adversarial loss is computed by the negative logarithm of the likelihood function for the discriminator's estimated probability that a generated instance

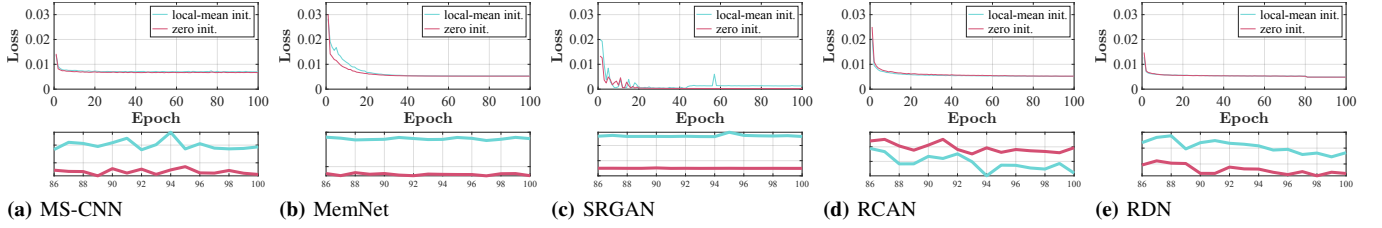


Fig. 6: Learning curves for zero and local-mean initialisation strategies over 100 epochs. Top plot shows training loss over 100 epochs. Bottom plot shows zoomed-in section from 86th to 100th epoch.

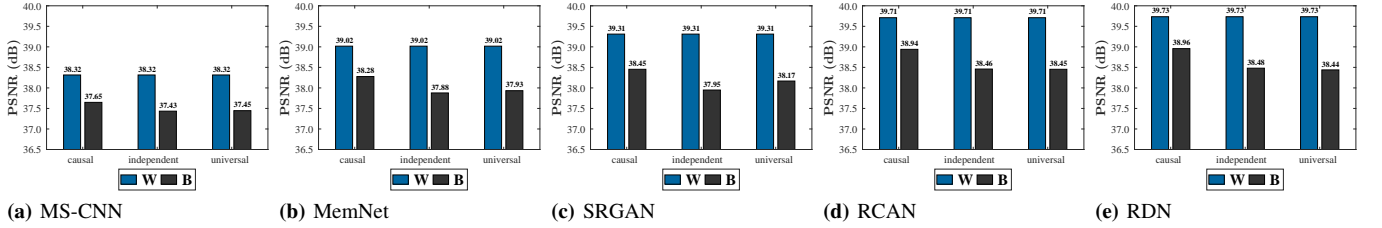


Fig. 7: Predictive accuracies of causal, independent, and universal training strategies for dual-layer prediction.

setting the pixel intensity to zero seems to be abrupt and oversimplified, this approach involves minimal intervention in the learning pipeline. It also has the virtue of low computational complexity. Hence, we adopt the zero initialisation strategy for the remaining experiments.

C. Comparison of Training Strategies

The predictive accuracies of the universal, independent, and causal training strategies for dual-layer prediction are depicted in Figure 7. The bars show the average PSNR scores between the ground-truth and predicted images w.r.t. different training strategies. As expected, the second-layer scores are generally lower than the first-layer scores due to the distributional shift. The causal training achieves a comparatively high accuracy for the second-layer prediction, whereas the performance gap between the other two strategies is not distinct. This suggests that the causal training using a training set with a distribution similar to that of the test set can alleviate the distributional shift to some extent. The narrow performance gap between the universal and independent training can be attributed to the translation-invariance property of CNNs. Although causal training requires additional computations when constructing the second training set, it is proved to be the most effective among the three training strategies. Hence, we opt for the causal training strategy for the remaining experiments.

D. Comparison of Model Efficiency

Model efficiencies are compared in Figure 8. The graph portrays the model size, represented by the number of trainable parameters, vis-à-vis the model accuracy, represented by the average PSNR score for the predicted images. The models are trained using the input/target pairs $(x_{\mathbb{B}}, x)$ and evaluated on the test set for the first-layer prediction. The trend suggests that model accuracy generally increases w.r.t. model size. While the statement that a deeper model works better does not hold

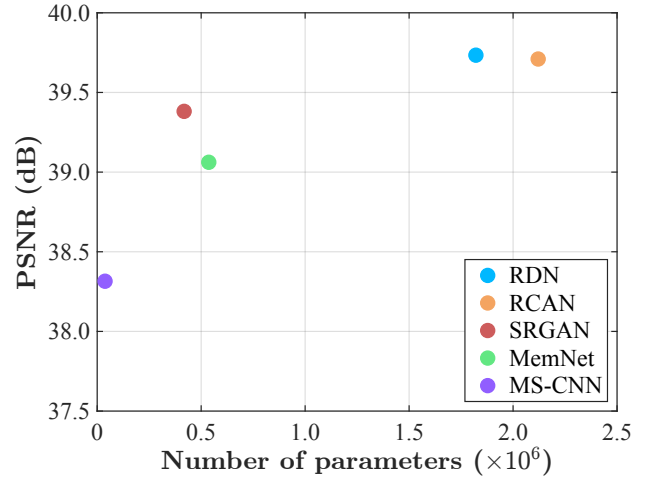


Fig. 8: Model efficiency represented by size vis-à-vis accuracy.

true for all cases, we can observe that the models with a size of around 2 million parameters (RDN and RCAN) achieve remarkably high accuracy in comparison with the two baseline models with a size of far less than 1 million parameters (MS-CNN and MemNet).

E. Evaluation of Visual Quality

Figure 9 depicts the ground-truth images selected from the BOSSbase and USC-SIPI datasets. Visual comparisons of different neural network models are shown in Figures 10 and 11. We evaluate the PSNR scores for images predicted from different neural network models. A close inspection of zoomed-in views reveals that deep models such as RCAN and RDN are better able to retrieve textural areas with reasonable accuracy when matched against the ground truth. By contrast, the SRGAN obtains moderate PSNR scores because its composite loss function does not directly optimise the pixel-wise loss. Compared with models oriented towards pixel-wise loss,

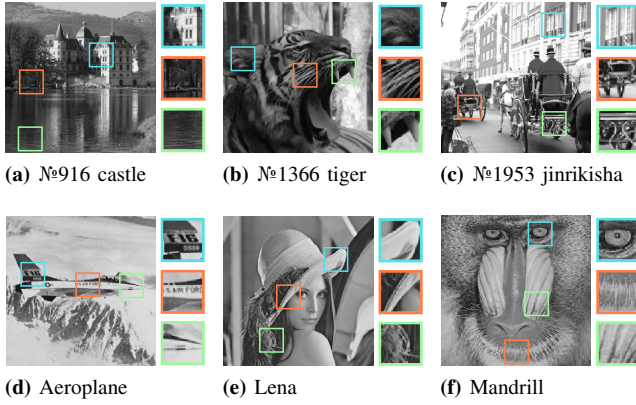


Fig. 9: Test images from BOSSbase (top row) and USC-SIPI (bottom row) datasets.

GAN-based models enjoy more flexibility in the sense that the generator may create new patterns to fit the distribution of natural images and thus outwit the discriminator, although this does not necessarily minimise the pixel-wise loss. The baseline models MS-CNN and MemNet, albeit inferior to the aforementioned models, manage to produce satisfactory results in comparison with the naïve LMI, owing to the ability of neural networks to learn rich patterns.

F. Evaluation of Distribution of Errors

The distribution of prediction errors plays a pivotal role in steganographic performance. Normally, errors would follow a Laplacian distribution and a more accurate model results in a more concentrated distribution. To analyse the error distribution, we examine the probability distribution function (PDF), cumulative distribution function (CDF), and Lorenz curve of errors, as shown in Figures 12, 13, and 14, respectively. We use the entropy, variance, percentile statistics, and Gini coefficient to measure the degree of error concentration [53]. Shannon’s entropy is maximised for a uniform distribution and the converse is equally true: a smaller entropy means a more concentrated distribution [54]. The variance is a measure of the spread of the data around the mean. The 95th percentile indicates the maximum error magnitude below which 95% of errors fall. The Gini coefficient is a measure of statistical dispersion intended to represent the inequality of the error magnitude within an image. A coefficient of 0 expresses perfect equality (dispersion), whereas a coefficient of 1 corresponds to maximal inequality (concentration). For the overall degree of concentration, the RDN and RCAN are ranked in the first tier, followed by the SRGAN, MemNet, and MS-CNN in the second tier, with the LMI ranked last.

G. Evaluation of Rate-Distortion Performance

The steganographic rate-distortion curves are plotted in Figure 15. The models with a higher predictive accuracy indeed achieve a better rate-distortion trade-off. The perceptual quality of stego images is inversely proportional to the embedding rate since distortions accumulate along the embedding process. A rise of ϑ increases the maximum embedding rate at the

cost of compromising the rate-distortion trade-off. Amongst all models, RCAN and RDN stand out, achieving state-of-the-art steganographic performance. Figure 16 displays stego images, their tonal distributions, and locations of carrier pixels w.r.t. different settings of stego-channel parameter ϑ . Results are generated by spreading a pseudo-random binary message over the whole image at the maximal steganographic capacity. It can be observed that the quality degradation is virtually imperceptible, the disturbance to the tonal distribution is subtle, and the pixels selected for carrying the payload are mostly clustered in smooth areas.

VI. CONCLUSION

Deep learning has revolutionised the research field of steganography and led to major technological breakthroughs in terms of capacity, imperceptibility, secrecy and robustness. It has also triggered interest in developing deep neural networks for reversible steganography. Whilst early studies demonstrated the potential of a joint encoder-decoder architecture to learn the steganographic system as a whole, this autonomous end-to-end framework suffers from imperfect reversibility due to an information bottleneck in neural networks. The lack of explainability in deep learning further exacerbates the issue. Modularisation is a reliable paradigm that divides a steganographic scheme into coding and analytics modules. Neural networks are employed in the analytics module to discover the underlying structures in images and learn to predict the intensity of a set of pixels (defined as the query) in the presence of another set of pixels (defined as the context). In this work, we have discussed unexplored issues such as the impact of intensity initialisation on predictive accuracy and the influence of distributional shift in dual-layer prediction. Experimental results have revealed that setting pixel intensity to zero, albeit seemingly arbitrary, renders a steadily low loss over several epochs. In addition, it has been found that training models in a causal way can, to some extent, ameliorate the distributional shift in deployment since it eliminates the discrepancy in the distributions of training and test sets. A comparative analysis has shown that advanced computer vision models outperform baseline models as well as a traditional non-neural model in terms of predictive accuracy and steganographic rate-distortion performance. We envision a promising paradigm shift in reversible steganography ushered in by deep learning and hope that this paper can prove instructive for future research.

ACKNOWLEDGEMENTS

This work was partially supported by the Japan Society for the Promotion of Science (JSPS) through KAKENHI Grants (JP16H06302, JP18H04120, JP20K23355, JP21H04907, and JP21K18023) and by the Japan Science and Technology Agency (JST) through CREST Grants (JPMJCR18A6 and JPMJCR20D3). The authors would like to thank the anonymous reviewers and the associate editor for their insightful comments and valuable suggestions that helped improve the quality of the article. Thanks to Anna Churchman for proofreading the article.



Fig. 10: Visual comparisons for selected BOSSbase images. Numerical data expresses PSNR (in dB).

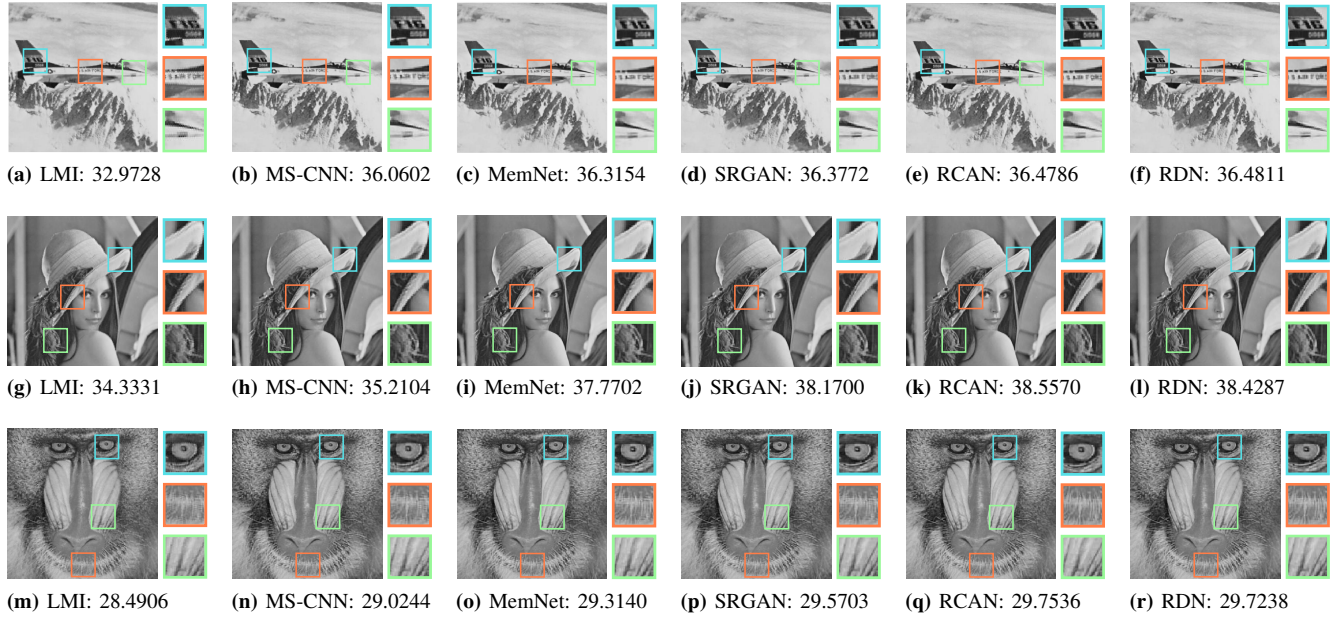


Fig. 11: Visual comparisons for selected USC-SIPI images. Numerical data expresses PSNR (in dB).

REFERENCES

- [1] A. M. Turing, "Computing machinery and intelligence," *Mind*, vol. LIX, no. 236, pp. 433–460, 1950.
- [2] Y. LeCun, Y. Bengio, and G. Hinton, "Deep learning," *Nature*, vol. 521, no. 7553, pp. 436–444, 2015.
- [3] J. Fridrich, M. Goljan, and R. Du, "Invertible authentication," in *Proc. SPIE Conf. Secur. Watermarking Multimedia Contents (SWMC)*, San Jose, CA, USA, 2001, pp. 197–208.
- [4] C. De Vleeschouwer, J.-F. Delaigle, and B. Macq, "Circular interpretation of bijective transformations in lossless watermarking for media asset management," *IEEE Trans. Multimedia*, vol. 5, no. 1, pp. 97–105, 2003.
- [5] J. Tian, "Reversible data embedding using a difference expansion," *IEEE Trans. Circuits Syst. Video Technol.*, vol. 13, no. 8, pp. 890–896, 2003.
- [6] M. U. Celik, G. Sharma, and A. M. Tekalp, "Lossless watermarking for image authentication: A new framework and an implementation," *IEEE Trans. Image Process.*, vol. 15, no. 4, pp. 1042–1049, 2006.
- [7] Z. Ni, Y.-Q. Shi, N. Ansari, and W. Su, "Reversible data hiding," *IEEE Trans. Circuits Syst. Video Technol.*, vol. 16, no. 3, pp. 354–362, 2006.
- [8] D. Coltuc, "Low distortion transform for reversible watermarking," *IEEE Trans. Image Process.*, vol. 21, no. 1, pp. 412–417, 2012.
- [9] G. Coatrieux, W. Pan, N. Cuppens-Boulahia, F. Cuppens, and C. Roux, "Reversible watermarking based on invariant image classification and dynamic histogram shifting," *IEEE Trans. Inf. Forensics Secur.*, vol. 8, no. 1, pp. 111–120, 2013.
- [10] Y.-Q. Shi, X. Li, X. Zhang, H. Wu, and B. Ma, "Reversible data hiding: Advances in the past two decades," *IEEE Access*, vol. 4, pp. 3210–3237, 2016.
- [11] I. Goodfellow, J. Shlens, and C. Szegedy, "Explaining and harnessing adversarial examples," in *Proc. Int. Conf. Learn. Represent. (ICLR)*, San

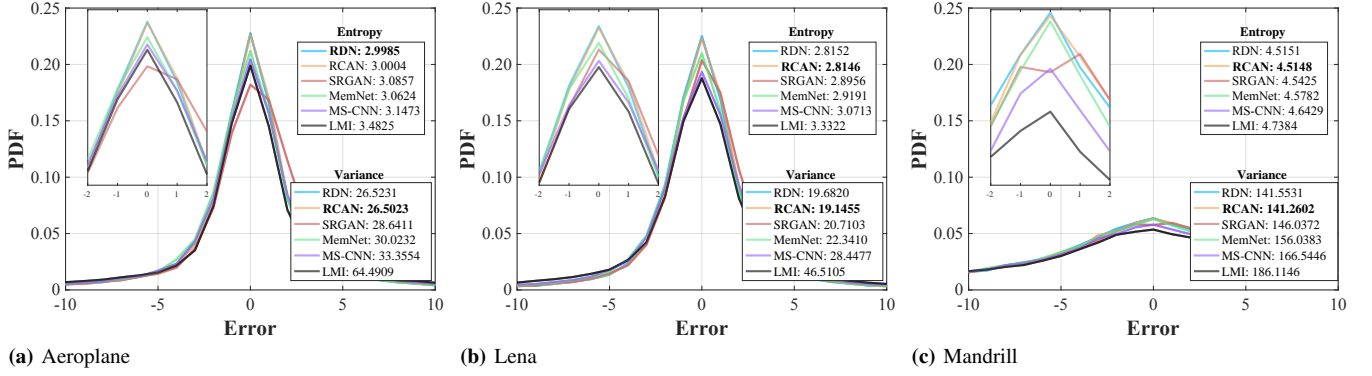


Fig. 12: Probability distribution function of errors. Numerical data expresses entropy and variance.

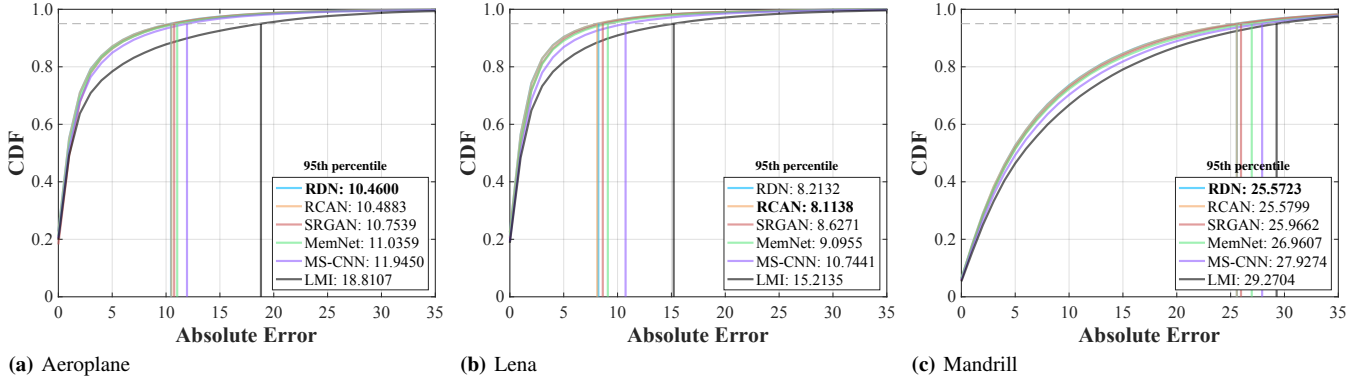


Fig. 13: Cumulative distribution function of errors. Numerical data expresses 95th percentile.

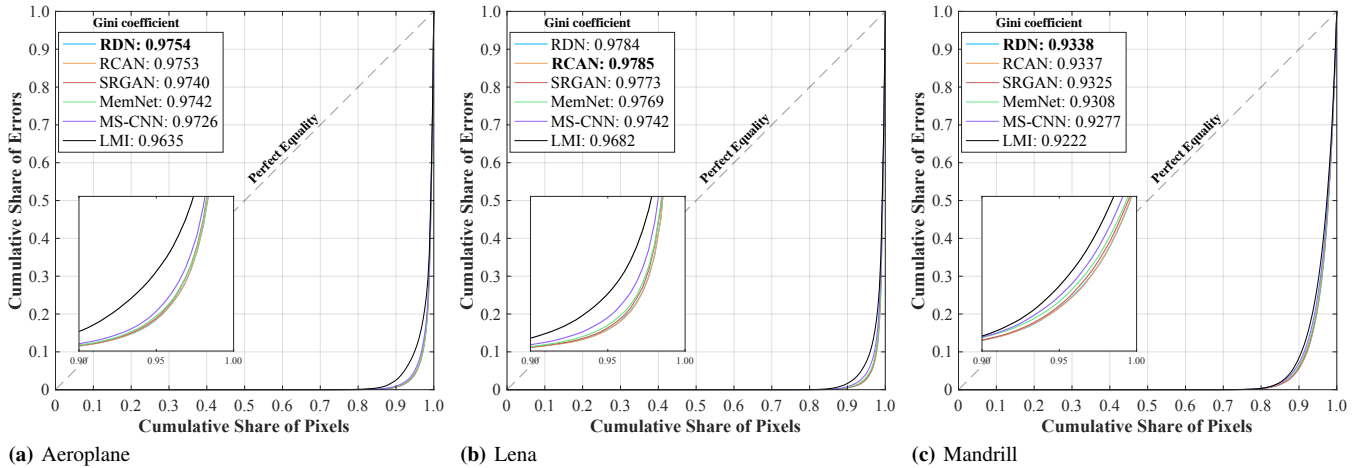


Fig. 14: Lorenz curve of errors. Numerical data expresses Gini coefficient.

- Diego, CA, USA, 2015, pp. 1–11.
- [12] S.-M. Moosavi-Dezfooli, A. Fawzi, and P. Frossard, “DeepFool: A simple and accurate method to fool deep neural networks,” in *Proc. IEEE Conf. Comput. Vis. Pattern Recognit. (CVPR)*, Las Vegas, NV, USA, 2016, pp. 2574–2582.
- [13] L. Muñoz González, B. Biggio, A. Demontis, A. Paudice, V. Wongrasamee, E. C. Lupu, and F. Roli, “Towards poisoning of deep learning algorithms with back-gradient optimization,” in *Proc. ACM Workshop Artif. Intell. Secur. (AISec)*, Dallas, TX, USA, 2017, pp. 27–38.
- [14] D. M. Thodi and J. J. Rodriguez, “Expansion embedding techniques for reversible watermarking,” *IEEE Trans. Image Process.*, vol. 16, no. 3, pp. 721–730, 2007.
- [15] M. Fallahpour, “Reversible image data hiding based on gradient adjusted prediction,” *IEICE Electron. Exp.*, vol. 5, no. 20, pp. 870–876, 2008.
- [16] X. Li, B. Yang, and T. Zeng, “Efficient reversible watermarking based on adaptive prediction-error expansion and pixel selection,” *IEEE Trans. Image Process.*, vol. 20, no. 12, pp. 3524–3533, 2011.
- [17] I. Dragoi and D. Coltuc, “Local prediction based difference expansion reversible watermarking,” *IEEE Trans. Image Process.*, vol. 23, no. 4, pp. 1779–1790, 2014.
- [18] H. J. Hwang, S. Kim, and H. J. Kim, “Reversible data hiding using least square predictor via the LASSO,” *EURASIP J. Image Video Process.*, vol. 2016, no. 1, pp. 42: 1–12, 2016.
- [19] R. Hu and S. Xiang, “CNN prediction based reversible data hiding,” *IEEE Signal Process. Lett.*, vol. 28, pp. 464–468, 2021.
- [20] C.-C. Chang, “Neural reversible steganography with long short-term memory,” *Secur. Commun. Netw.*, vol. 2021, pp. 5 580 272:1–14, 2021.
- [21] Y. Tai, J. Yang, X. Liu, and C. Xu, “MemNet: A persistent memory network for image restoration,” in *Proc. IEEE Int. Conf. Comput. Vis. (ICCV)*, Venice, Italy, 2017, pp. 4549–4557.
- [22] C. Ledig, L. Theis, F. Huszár, J. Caballero, A. Cunningham, A. Acosta, A. Aitken, A. Tejani, J. Totz, Z. Wang, and W. Shi, “Photo-realistic

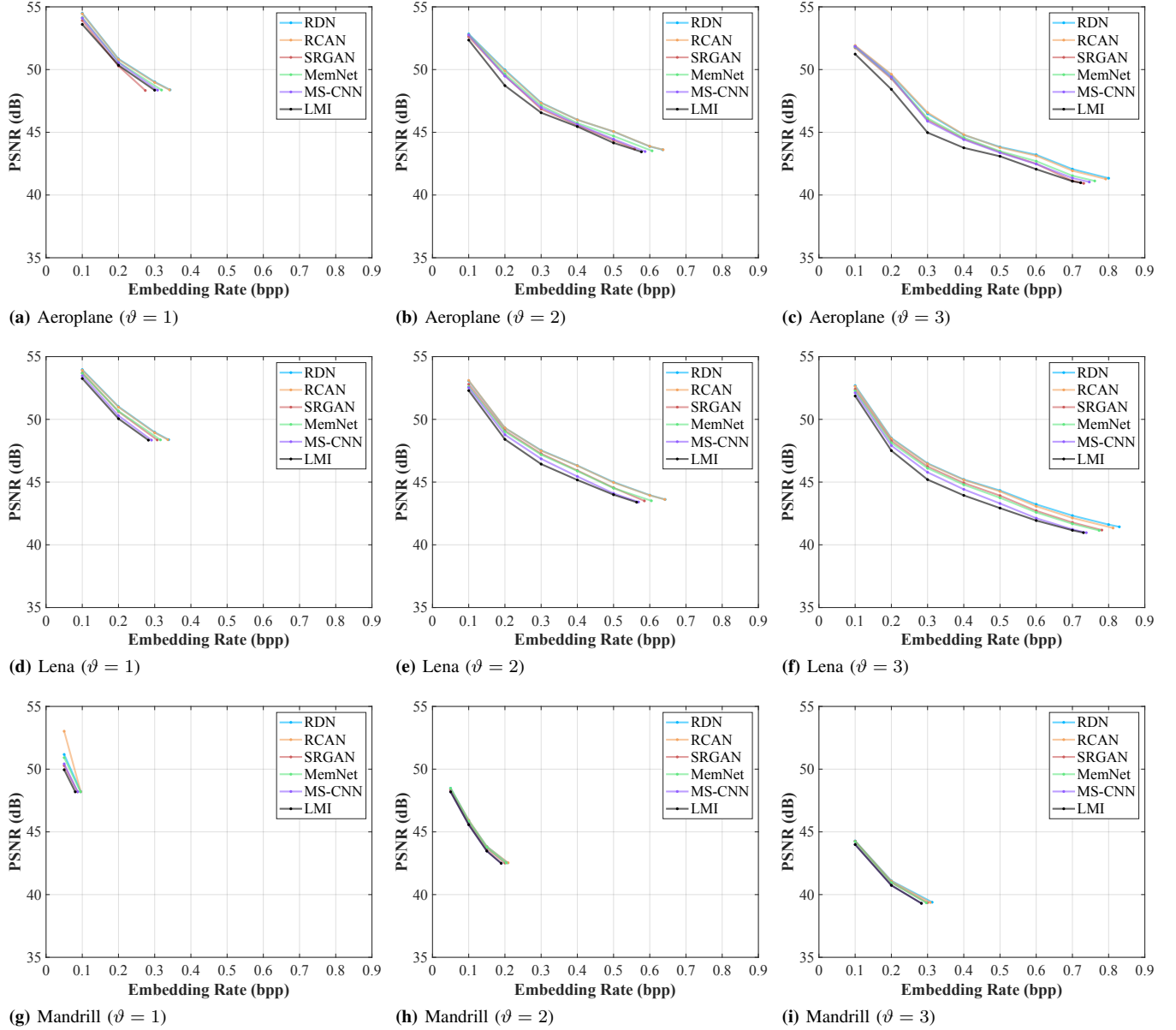


Fig. 15: Rate-distortion curves for different settings of stego-channel parameter ϑ .

- single image super-resolution using a generative adversarial network,” in *Proc. IEEE Conf. Comput. Vis. Pattern Recognit. (CVPR)*, Honolulu, HI, USA, 2017, pp. 105–114.
- [23] Y. Zhang, K. Li, K. Li, L. Wang, B. Zhong, and Y. Fu, “Image super-resolution using very deep residual channel attention networks,” in *Proc. Eur. Conf. Comput. Vis. (ECCV)*, Munich, Germany, 2018, pp. 294–310.
- [24] Y. Zhang, Y. Tian, Y. Kong, B. Zhong, and Y. Fu, “Residual dense network for image super-resolution,” in *Proc. IEEE/CVF Conf. Comput. Vis. Pattern Recognit. (CVPR)*, Salt Lake City, UT, USA, 2018, pp. 2472–2481.
- [25] J. Zhu, R. Kaplan, J. Johnson, and L. Fei-Fei, “HiDDeN: Hiding data with deep networks,” in *Proc. Eur. Conf. Comput. Vis. (ECCV)*, Munich, Germany, 2018, pp. 682–697.
- [26] W. Tang, S. Tan, B. Li, and J. Huang, “Automatic steganographic distortion learning using a generative adversarial network,” *IEEE Signal Process. Lett.*, vol. 24, no. 10, pp. 1547–1551, 2017.
- [27] W. Tang, B. Li, S. Tan, M. Barni, and J. Huang, “CNN-based adversarial embedding for image steganography,” *IEEE Trans. Inf. Forensics Secur.*, vol. 14, no. 8, pp. 2074–2087, 2019.
- [28] J. Yang, D. Ruan, J. Huang, X. Kang, and Y.-Q. Shi, “An embedding cost learning framework using GAN,” *IEEE Trans. Inf. Forensics Secur.*, vol. 15, pp. 839–851, 2020.
- [29] D. Volkhonskiy, I. Nazarov, and E. Burnaev, “Steganographic generative adversarial networks,” in *Proc. Int. Conf. Mach. Vis. (ICMV)*, vol. 11433, Amsterdam, Netherlands, 2019, pp. 1–15.
- [30] J. Hayes and G. Danezis, “Generating steganographic images via adversarial training,” in *Proc. Adv. Neural Inf. Process. Syst. (NeurIPS)*, Long Beach, CA, USA, 2017, pp. 1951–1960.
- [31] D. Hu, L. Wang, W. Jiang, S. Zheng, and B. Li, “A novel image steganography method via deep convolutional generative adversarial networks,” *IEEE Access*, vol. 6, pp. 38 303–38 314, 2018.
- [32] X. Luo, R. Zhan, H. Chang, F. Yang, and P. Milanfar, “Distortion agnostic deep watermarking,” in *Proc. IEEE/CVF Conf. Comput. Vis. Pattern Recognit. (CVPR)*, Seattle, WA, USA, 2020, pp. 13 545–13 554.
- [33] E. Wengrowski and K. Dana, “Light field messaging with deep photographic steganography,” in *Proc. IEEE Conf. Comput. Vis. Pattern Recognit. (CVPR)*, Long Beach, CA, USA, 2019, pp. 1515–1524.
- [34] H. Fang, D. Chen, F. Wang, Z. Ma, H. Liu, W. Zhou, W. Zhang, and N. H. Yu, “TERA: Screen-to-camera image code with transparency, efficiency, robustness and adaptability,” *IEEE Trans. Multimedia*, pp. 1–13, 2021.
- [35] M. Tancik, B. Mildenhall, and R. Ng, “StegaStamp: Invisible hyperlinks

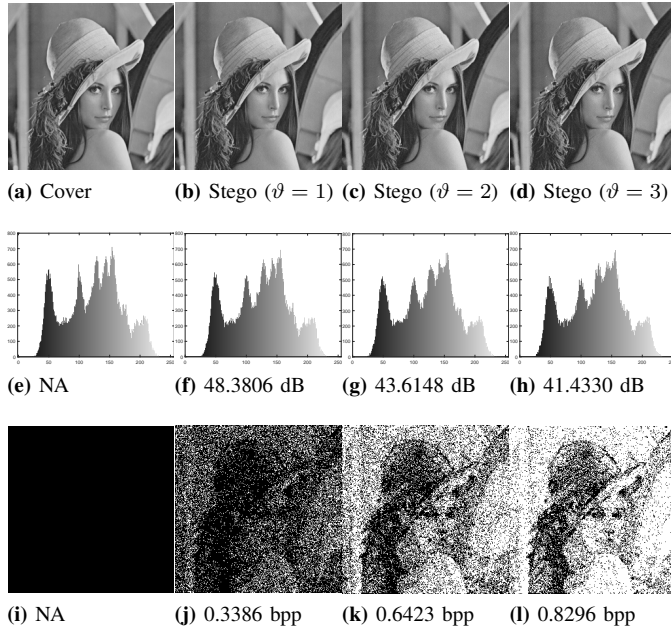


Fig. 16: Stego images, their tonal distributions, and locations of carrier pixels (coloured in white). Numerical data expresses PSNR and embedding rate.

- in physical photographs,” in *Proc. IEEE/CVF Conf. Comput. Vis. Pattern Recognit. (CVPR)*, Seattle, WA, USA, 2020, pp. 2114–2123.
- [36] X. Duan, K. Jia, B. Li, D. Guo, E. Zhang, and C. Qin, “Reversible image steganography scheme based on a U-Net structure,” *IEEE Access*, vol. 7, pp. 9314–9323, 2019.
- [37] K.-H. Jung, Z. Zhang, G. Fu, F. Di, C. Li, and J. Liu, “Generative reversible data hiding by image-to-image translation via GANs,” *Secur. Commun. Netw.*, vol. 2019, pp. 4932782:1–10, 2019.
- [38] S.-P. Lu, R. Wang, T. Zhong, and P. L. Rosin, “Large-capacity image steganography based on invertible neural networks,” in *Proc. IEEE/CVF Conf. Comput. Vis. Pattern Recognit. (CVPR)*, virtual, 2021, pp. 10816–10825.
- [39] J. Fridrich, M. Goljan, and R. Du, “Lossless data embedding—New paradigm in digital watermarking,” *EURASIP J. Adv. Signal Process.*, vol. 986842, no. 2002, pp. 185–196, 2002.
- [40] C.-C. Chang, “Adversarial learning for invertible steganography,” *IEEE Access*, vol. 8, pp. 198425–198435, 2020.
- [41] P. Isola, J.-Y. Zhu, T. Zhou, and A. A. Efros, “Image-to-image translation with conditional adversarial networks,” in *Proc. IEEE Conf. Comput. Vis. Pattern Recognit. (CVPR)*, Honolulu, HI, USA, 2017, pp. 5967–5976.
- [42] V. Sachnev, H. J. Kim, J. Nam, S. Suresh, and Y.-Q. Shi, “Reversible watermarking algorithm using sorting and prediction,” *IEEE Trans. Circuits Syst. Video Technol.*, vol. 19, no. 7, pp. 989–999, 2009.
- [43] E. B. Wilson, “First and second laws of error,” *J. Amer. Statist. Assoc.*, vol. 18, no. 143, pp. 841–851, 1923.
- [44] A. L. Maas, A. Y. Hannun, and A. Y. Ng, “Rectifier nonlinearities improve neural network acoustic models,” in *Proc. Int. Conf. Mach. Learn. (ICML)*, Atlanta, GA, USA, 2013, pp. 1–6.
- [45] X. Glorot, A. Bordes, and Y. Bengio, “Deep sparse rectifier neural networks,” in *Proc. Int. Conf. Artif. Intell. Statist. (AISTATS)*, Fort Lauderdale, FL, USA, 2011, pp. 315–323.
- [46] K. He, X. Zhang, S. Ren, and J. Sun, “Delving deep into rectifiers: Surpassing human-level performance on imagenet classification,” in *Proc. IEEE Int. Conf. Comput. Vis. (ICCV)*, Santiago, Chile, 2015, pp. 1026–1034.
- [47] K. Simonyan and A. Zisserman, “Very deep convolutional networks for large-scale image recognition,” in *Proc. Int. Conf. Learn. Represent. (ICLR)*, San Diego, CA, USA, 2015, pp. 1–14.
- [48] P. Bas, T. Filler, and T. Pevný, “Break our steganographic system: The ins and outs of organizing BOSS,” in *Proc. Int. Workshop Inf. Hiding (IH)*, Prague, Czech Republic, 2011, pp. 59–70.
- [49] C. Szegedy, Wei Liu, Yangqing Jia, P. Sermanet, S. Reed, D. Anguelov, D. Erhan, V. Vanhoucke, and A. Rabinovich, “Going deeper with

convolutions,” in *Proc. IEEE Conf. Comput. Vis. Pattern Recognit. (CVPR)*, Boston, MA, USA, 2015, pp. 1–9.

- [50] O. Russakovsky, J. Deng, H. Su, J. Krause, S. Satheesh, S. Ma, Z. Huang, A. Karpathy, A. Khosla, M. Bernstein, A. C. Berg, and L. Fei-Fei, “ImageNet large scale visual recognition challenge,” *Int. J. Comput. Vis.*, vol. 115, no. 3, pp. 211–252, 2015.
- [51] C. E. Duchon, “Lanczos filtering in one and two dimensions,” *J. Appl. Meteorol.*, vol. 18, no. 8, pp. 1016–1022, 1979.
- [52] A. G. Weber, “The USC-SIPI image database: Version 5,” USC Viterbi School Eng., Signal Image Process. Inst., Los Angeles, CA, USA, Tech. Rep. 315, 2006.
- [53] P. E. Hart, “Entropy and other measures of concentration,” *J. Roy. Statist. Soc. Ser. A*, vol. 134, no. 1, pp. 73–85, 1971.
- [54] C. E. Shannon, “A mathematical theory of communication,” *Bell Syst. Tech. J.*, vol. 27, no. 3, pp. 379–423, 1948.

PLACE
PHOTO
HERE

Ching-Chun Chang received his Ph.D. in Computer Science from the University of Warwick, UK, in 2019. He engaged in a short-term scientific mission supported by European Cooperation in Science and Technology Actions at the Faculty of Computer Science, Otto-von-Guericke-Universität Magdeburg, Germany, in 2016. He was granted the Marie-Curie fellowship and participated in a research and innovation staff exchange scheme supported by Marie Skłodowska-Curie Actions at the Department of Electrical and Computer Engineering, New Jersey Institute of Technology, USA, in 2017. He was a Visiting Scholar with the School of Computer and Mathematics, Charles Sturt University, Australia, in 2018, and with the School of Information Technology, Deakin University, Australia, in 2019. He was a Research Fellow with the Department of Electronic Engineering, Tsinghua University, China, in 2020. He is currently a Postdoctoral Fellow with the National Institute of Informatics, Japan. His research interests include steganography, watermarking, forensics, biometrics, cybersecurity, applied cryptography, image processing, computer vision, natural language processing, computational linguistics, machine learning and artificial intelligence.

PLACE
PHOTO
HERE

Xu Wang received his M.S. degree in Information Science from Central China Normal University in 2018. He is currently pursuing his Ph.D. degree in Information Engineering and Computer Science, at Feng Chia University, Taichung, Taiwan. His research interests include image and signal processing, multimedia security and information hiding.

PLACE
PHOTO
HERE

Sisheng Chen received his B.S. degree from Shan Dong University, in 2005, and his M.S. degree in Applied Mathematics from Fujian Normal University, in 2008. He is currently pursuing his Ph.D. degree in Information Engineering and computer science, at Feng Chia University, Taichung, Taiwan. He is also a Lecturer with the Fujian Polytechnic Normal University. His research interests include multimedia security and wireless network security.

PLACE
PHOTO
HERE

Isao Echizen received B.S., M.S. and D.E. degrees from Tokyo Institute of Technology, Japan, in 1995, 1997 and 2003, respectively. He joined Hitachi, Ltd. in 1997, and until 2007, he was a Research Engineer in the company's Systems Development Laboratory. He was a Visiting Professor with the University of Freiburg in 2010 and with the University of Halle-Wittenberg in 2011. He is currently the Deputy Director General of the National Institute of Informatics (NII), a Professor with the Information and Society Research Division, NII, and a Professor with

the Graduate School of Information Science and Technology, Department of Information and Communication Engineering, University of Tokyo. He is also a Visiting Professor with Tsuda University. He has been engaged in research on information security and content security and privacy. He is a member of the Information Forensics and Security Technical Committee and the IEEE Signal Processing Society. He received the Best Paper Award from the IPSJ in 2005 and 2014, the Fujio Frontier Award and the Image Electronics Technology Award in 2010, the One of the Best Papers Award from the Information Security and Privacy Conference and the IPSJ Nagao Special Researcher Award in 2011, the Docomo Mobile Science Award in 2014, the Information Security Cultural Award in 2016, and the Best Paper Award at the IEEE WIFS 2017.

PLACE
PHOTO
HERE

Victor Sanchez received his M.Sc. degree from the University of Alberta, Canada, in 2003, and his Ph.D. degree from the University of British Columbia, Canada, in 2010. From 2011 to 2012, he was with the Video and Image Processing Laboratory, University of California at Berkeley, as a Postdoctoral Researcher. In 2012, he was a Visiting Lecturer with the Group on Interactive Coding of Images, Universitat Autònoma de Barcelona. From 2018 to 2019, he was a Visiting Scholar with the School of Electrical and Information Engineering,

University of Sydney, Australia. He is currently an Associate Professor with the Department of Computer Science, University of Warwick, UK. His research has been funded by the Consejo Nacional de Ciencia y Tecnología, Mexico, the Natural Sciences and Engineering Research Council of Canada, the Canadian Institutes of Health Research, the FP7 and the H2020 Programs of the European Union, the Engineering and Physical Sciences Research Council, UK, and the Defence and Security Accelerator, UK. He has authored several technical articles, book chapters and a book in these areas. His main research interests include signal and information processing with applications to multimedia analysis, image and video coding, security and communications.

PLACE
PHOTO
HERE

Chang-Tsun Li received his B.Sc. degree in Electrical Engineering from the National Defence University, Taiwan, in 1987, his M.Sc. degree in Computer Science from the US Naval Postgraduate School, USA, in 1992, and his Ph.D. degree in Computer Science from the University of Warwick, UK, in 1998. He was an Associate Professor with the Department of Electrical Engineering, National Defence University, from 1998 to 2002, and also a Visiting Professor with the Department of Computer Science, US Naval Postgraduate School, in 2001.

He was a Professor with the Department of Computer Science, University of Warwick, UK, on a full-time basis until 2017 and is still affiliated with Warwick on a part-time basis. He was also a Professor with Charles Sturt University, Australia, from 2017 to 2019. He is currently a Professor of cyber security with the School of Information Technology, Deakin University, Australia, where he is also a Research Director with the Centre for Cyber Security Research and Innovation. His research interests include multimedia forensics and security, biometrics, machine learning, data analytics, computer vision, image processing, pattern recognition, bioinformatics and content-based image retrieval. His research outcomes have been translated into award-winning commercial products protected by a series of international patents and have been used by a number of institutions in the law enforcement, national security, banking and commercial sectors around the world. He is currently an Associate Editor of IEEE ACCESS, EURASIP Journal of Image and Video Processing (JIVP) and IET Biometrics. He has been involved in the organisation of many international conferences and workshops and also served as member of the international program committees for several international conferences. He is also actively contributing keynote speeches and talks at various international events.